Title:
**Unified and Efficient Approach for Extracting Reflection-Symmetry Regions from 3D CAD Models Containing Free-Form Surfaces**

Authors:
Ren Nakata, r-nakata-2000@eis.hokudai.ac.jp, Hokkaido University
Satoshi Kanai, kanai@ssi.ist.hokudai.ac.jp, Hokkaido University
Hiroaki Date, hdate@ssi.ist.hokudai.ac.jp, Hokkaido University
Hideyoshi Takashima, hideyoshi_takashima@ais-hokkaido.co.jp, AIS Hokkaido, Inc.
Tetsufumi Taichi, tetsufumi_taichi@ais-hokkaido.co.jp, AIS Hokkaido, Inc.

Keywords:
Symmetry, Solid Model, CAD, Free-form Surface, Curvature, Finite-element Mesh

DOI: 10.14733/cadconfP.2024.152-157

Introduction:

In recent years, the cost of computer-aided engineering (CAE) model creation while developing automotive products has increased. Shortening the time required to create such models is essential. During CAE model creation, generating a finite-element (FE) mesh that meets the analysis specifications from a solid product model is necessary. When there are geometrically symmetric portions in a solid model, an FE mesh can be efficiently generated by ensuring that it conforms to the specifications only for the reference portion and copying the mesh for the remaining symmetric portions. However, extracting symmetric portions from the model currently relies on manual work by CAE engineers, which is time-consuming and prone to oversights. Therefore, there is a strong need for an algorithm that can automatically extract symmetry regions from a solid model and present them to the user. Furthermore, the solid models of automotive parts made through casting and forging comprise planar and cylindrical surfaces as well as free-form surfaces such as nonuniform rational B-spline (NURBS), revolution, and extrusion surfaces. Therefore, the algorithm must detect symmetry regions that contain a mixture of such analytical and free-form surfaces. Moreover, symmetry region extraction must be efficient enough to handle the tens of thousands of faces in large-scale solid models of automotive parts.

Many studies are already available on algorithms for extracting symmetric regions from solid models, such as [1]-[3]. However, [2] and [3] did not mention the applicability to models containing free-form surfaces or provide examples of extraction for symmetric free-form surfaces. [1] presents a method for symmetry region estimation by comparing the mass properties of faces, such as areas and centers of gravity, and is fast in extraction. However, this method verifies only the necessary condition of symmetry between faces and does not verify the sufficient condition that requires a test of geometric symmetry between faces. In contrast, methods [4] and [6] have been proposed to extract symmetry regions from triangular meshes or point clouds. However, these methods show problems in the degradation of representation resolution because of discretization from solid models to meshes or point clouds and in processing efficiency for large-scale solid models.

This research proposes an algorithm that can extract reflection-symmetry regions on solid models, including free-form surfaces, in a uniform and efficient manner. “Uniform” means that the principal curvature distribution on the face is used as the primary descriptor to provide a symmetry test independent of the geometric class of the faces in a solid model. Meanwhile, “efficient” means that hierarchical filtering and the random sample consensus (RANSAC) algorithm reduce the time-consuming geometric symmetry test between faces. The proposed algorithm can extract symmetry regions in less than a few milliseconds per face.

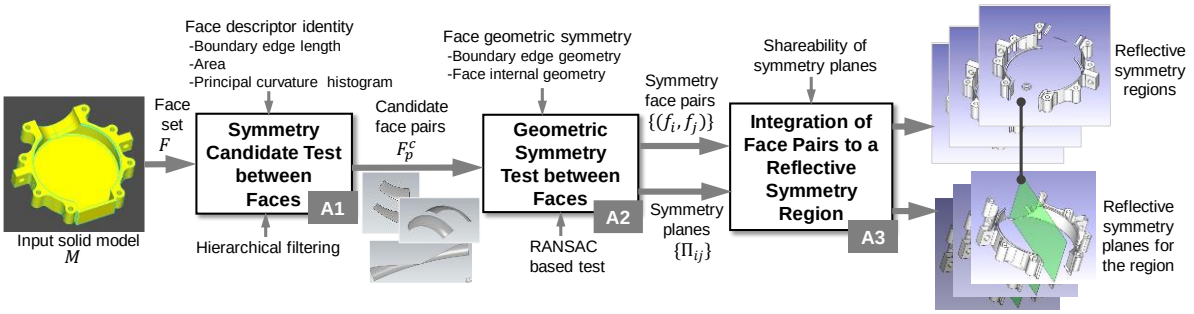


Fig. 1: Processing pipeline of the proposed reflection symmetry region extraction.

Method for Extracting Reflection-symmetry Regions:

*Overview*

Fig. 1. shows the processing pipeline of the proposed reflection-symmetry region extraction process. The process comprises the symmetry candidate test performed between faces (A1), the geometric symmetry test of the candidate face pair (A2), and the integration of symmetric face pairs to a symmetry region (A3). In A1, for every face pair in an input solid model, the necessary condition of the face-to-face reflection symmetry is tested using hierarchical filtering. Then, in A2, the sufficient condition is tested by examining the symmetry of boundary edges and internal geometries between the faces of the candidate face pair. If the test is passed, corresponding symmetry planes are estimated. Finally, in A3, face pairs that share a symmetry plane are clustered to generate a reflection-symmetry region.

In hierarchical filtering of A1, we do not compare geometry class labels of the underlying surfaces of face pairs to be tested (e.g., "*Cylindrical surface*" and "*B-spline surface*") and the class-dependent intrinsic parameters (e.g., the radius of the cylindrical surface). Instead, we compare only the descriptor values common to all faces: boundary edge lengths, areas, and principal curvature distributions of the face pair. Therefore, symmetry can be judged in a unified manner for cases where the actual geometries are symmetrical. However, the apparent geometry classes of the faces are different. The process can work even for solid models that include NURB, revolution, and extrusion surfaces. The following subsections describe the processing pipeline in more detail.

*Symmetry Candidate Test Between Faces Using Hierarchical Filtering*

The test first retrieves the set of all faces $F = \{f_i\}$ in an input solid model $M$, hierarchically examines the necessary conditions of face-to-face reflection symmetry $Nc(f_i, f_j) \in \{true, false\}$ for all face combinations $\forall(f_i, f_j) \in F \times F$, and extracts a set of candidate symmetric face pair $F_p^c = \{(f_i, f_j) | (f_i, f_j) \in F \times F, Nc(f_i, f_j) = true\}$. The efficiency of this test is improved by checking only the identity between descriptor values of the faces and by eliminating asymmetric face pairs earlier in the following hierarchical manner.

(1) The number of vertices $d_{nv}$ and boundary edge length $d_{bl}$ of each face are compared for a pair of faces $(f_i, f_j)$. If $d_{nv}(f_i) = d_{nv}(f_j)$ and $d_{bl}(f_i) = d_{bl}(f_j)$, proceed to step (2). Otherwise, the pair $(f_i, f_j)$ is judged asymmetric.

(2) Area of each face, $d_{ar}$, are compared. If $d_{ar}(f_i) = d_{ar}(f_j)$, proceed to step (3). Otherwise, the pair $(f_i, f_j)$ is judged asymmetric.

(3) The principal curvature histogram, $d_{ch}$, described below is evaluated for each face. If the histograms $d_{ch}(f_i)$ and $d_{ch}(f_j)$ are consistent, the face pair $(f_i, f_j)$ is inserted into the set of symmetric face pair candidates, $F_p^c$. Otherwise, the pair $(f_i, f_j)$ is judged asymmetric.

*Principal Curvature Histogram for a Symmetric Face Pair Candidate*

In the last step of the symmetry candidate test, we use the property that the statistical distributions of the principal curvatures on two faces are consistent if the two faces are reflection symmetric. This property can make the test independent of the geometry class of the face. The principal curvature histogram is introduced to encode the curvature distribution. The evaluation of the principal curvature histogram is implemented on Open CASCADE [5]. In Open CASCADE, every geometry of a face in a solid

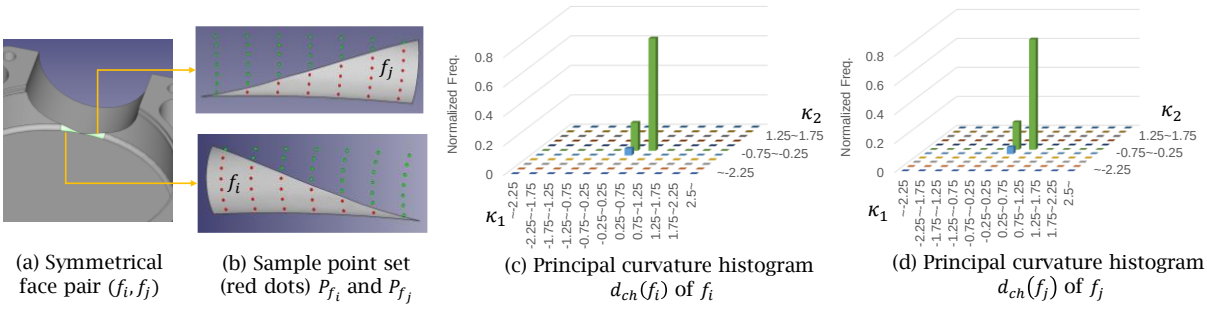


(a) Symmetrical face pair $(f_i, f_j)$ (b) Sample point set (red dots) $P_{f_i}$ and $P_{f_j}$ (c) Principal curvature histogram $d_{ch}(f_i)$ of $f_i$ (d) Principal curvature histogram $d_{ch}(f_j)$ of $f_j$

Fig. 2: Principal curvature histogram of a symmetrical face pair.

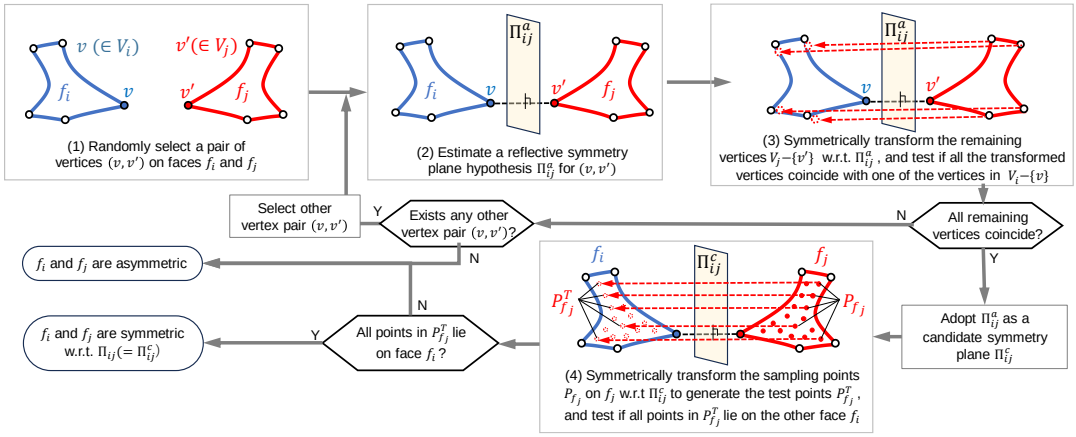


Fig. 3: Flow of the geometric symmetry test between faces.

model, even if it is an analytic surface, for example, a cylindrical one, is uniformly defined as a parametric form of Eqn.(1):

$$\boldsymbol{p}(u,v) = [p_x(u,v), \quad p_y(u,v), \quad p_z(u,v)] \in \mathcal{R}^3, \tag{1}$$

where $\boldsymbol{p}(u,v)$ represents a 3-dimensional point on the surface at the parameter $(u,v)$. From Eqn.(1), the first and second derivatives of the surface $\partial\boldsymbol{p}/\partial u$, $\partial\boldsymbol{p}/\partial v$, $\partial^2\boldsymbol{p}/\partial u^2$, $\partial^2\boldsymbol{p}/\partial v^2$, and $\partial^2\boldsymbol{p}/\partial u\partial v$ can be analytically and efficiently evaluated at $\boldsymbol{p}(u,v)$. Then, from a simple calculation in differential geometry, the principal curvatures $\kappa_1$ and $\kappa_2$ $(\kappa_1 \geq \kappa_2)$ at $\boldsymbol{p}(u,v)$ can be obtained from the first and second fundamental forms.

For constructing the principal curvature histogram $d_{ch}(f)$ of a face $f$, we first generate the sampling parameter set $D_f = \{(u_i, v_i)\}$ at regular intervals over $(u,v)$ domain of $f$ and produce the sample points $P_f = \{\boldsymbol{p}(u_i, v_i) \,|(u_i, v_i) \in D_f\}$ for $f$. Next, the principal curvature $\kappa_1(u_i, v_i)$ and $\kappa_2(u_i, v_i)$ values are discretely classified into the intervals $I_1^{\kappa 1}, I_2^{\kappa 1}, \cdots, I_{J1}^{\kappa 1}$ and $I_1^{\kappa 2}, I_2^{\kappa 2}, \cdots, I_{J2}^{\kappa 2}$ respectively. A two-dimensional principal curvature histogram $d_{ch}(f)$ is then constructed, as shown in Eqn.(2):

$$d_{ch}(f) = \left\{ q(l,m) \mid \kappa_1(u_i, v_i) \in I_l^{\kappa 1},\ \kappa_2(u_i, v_i) \in I_m^{\kappa 2},\ \forall (u_i, v_i) \in D_f, l \in [1, J_1], m \in [1, J_2] \right\}, \tag{2}$$

where $q(l,m)$ denotes the number of the sample points and $\kappa_1$ and $\kappa_2$ values are contained in the intervals $I_l^{\kappa 1}$and $I_m^{\kappa 2}$ divided by $|D_f|$. Fig. 2. illustrates examples of principal curvature histograms.

Finally, for a face pair $(f_i, f_j)$, the histogram intersection $H_{ch}(f_i, f_j)$ between $d_{ch}(f_i)$ and $d_{ch}(f_j)$ are evaluated. If $H_{ch}(f_i, f_j)$ is greater than the threshold, we judge the curvature distribution of $f_i$ and $f_j$ match, and the pair $(f_i, f_j)$ is then inserted into the set of symmetric face pair candidates $F_p^c$.

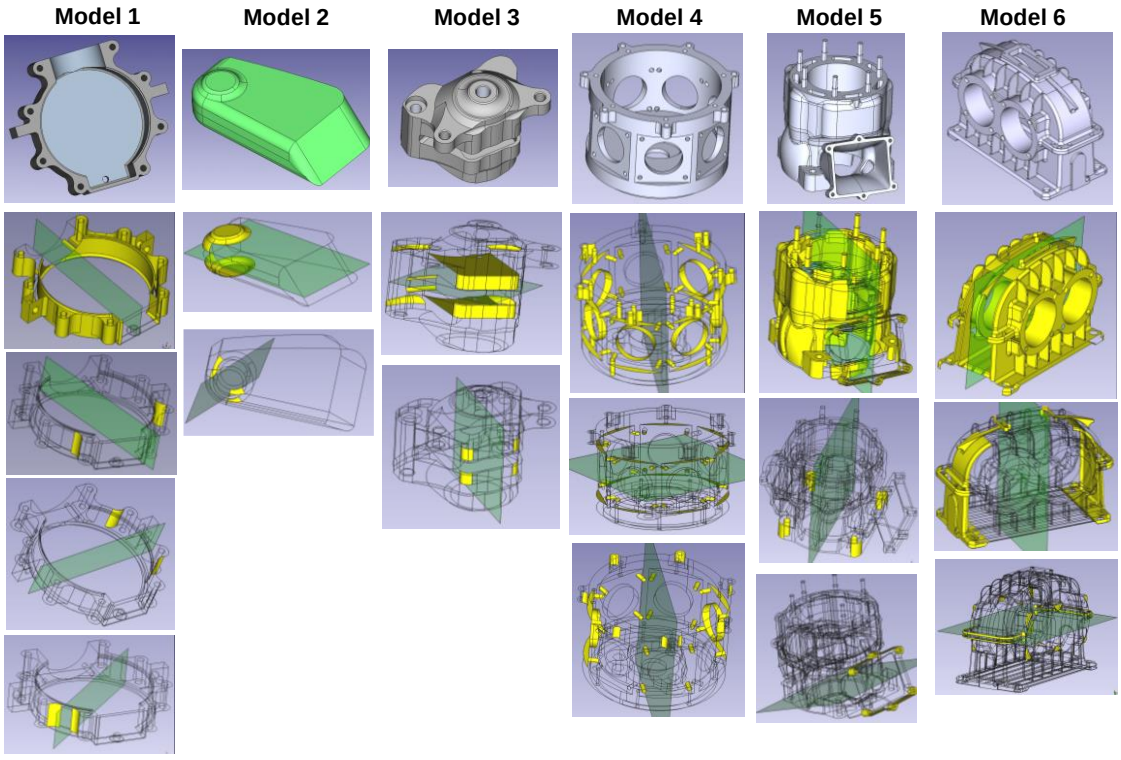


Fig. 4: Examples of the extraction of reflection symmetry regions (yellow) with symmetry planes (green). For models 1, 4, 5 and 6, only a part of the symmetry regions are shown.

*Geometric Symmetry Test Between Faces*

The symmetry of boundary edges and internal geometries is tested between faces in the symmetric face pair candidates $(f_i, f_j) \in F_p^c$ as a last step. In the test, we assume that a vertex always exists on the other face in a reflection-symmetric relation to a vertex on one face. Fig. 3. Shows the flow of the geometric symmetry test. The following RANSAC-based algorithm (1)-(4) is adopted for the test:

(1) A pair of vertices $(v, v')$ $(v \in V_i,\ v' \in V_j)$ is randomly selected from $V_i$ and $V_j$.

(2) The bisecting plane between $(v, v')$ is estimated as a symmetry plane hypothesis $\Pi_{ij}^a$.

(3) Every vertex in $V_j - \{v'\}$ is symmetrically transformed with respect to $\Pi_{ij}^a$, and its transformed position is tested if it coincides with one of the vertices in $V_i - \{v\}$. If all vertices in $V_j - \{v'\}$ pass the test, the plane $\Pi_{ij}^a$ is adopted as a candidate symmetry plane $\Pi_{ij}^c$ and proceed to step(4). Otherwise, the selection of $v'$ from $V_j$ is changed, and the process is repeated from (2). If the test does not pass for any vertex pair, the face pair $(f_i, f_j)$ is determined to be asymmetric.

(4) A set of sampling points $P_{f_j} = \{\boldsymbol{p}(u,v) \,|(u,v) \in D_{f_j}\}$ generated on a face to be tested $f_j$ are symmetrically transformed to points $P_{f_j}^T$ concerning $\Pi_{ij}^c$, and the projected distance of every point in $P_{f_j}^T$ onto the other face $f_i$ is evaluated. If the maximum of these distances is within the threshold, then the geometry of $(f_i, f_j)$ are determined to be reflection-symmetric w.r.t. the symmetry plane $\Pi_{ij}$ $(= \Pi_{ij}^c)$.

Case Study:

The validity of the proposed algorithm was verified using six small and medium-scale solid models, including not only analytic surfaces, however, free-form surfaces such as NURB and revolution surfaces, as shown in Fig. 4. Based on preliminary experiments, the number of the sampling parameters on $(u, v)$ domain $|D_f|$ was set to $7 \times 7$. The numbers of classification intervals in the histogram ($J_1$ and $J_2$) were set

to 11. The identity thresholds for the boundary edge length and area comparisons were set to 0.01 mm and 0.01 mm$^2$. The distance threshold for the geometric symmetry test was set to 0.01 mm. Fig. 4. shows examples of some of the extracted symmetric regions and their symmetry planes. A visual inspection of

| | *Model 1* | *Model 2* | *Model 3* | *Model 4* | *Model 5* | *Model 6* |
|---|---|---|---|---|---|---|
| Approx. model size (W×D×H) [mm] | 200×227 ×14 | 18×10 ×5 | 76×55 ×65 | 107×107 ×63 | 139×139 ×140 | 300×145 ×197 |
| # of faces | 130 | 37 | 167 | 271 | 1291 | 1598 |
| # of extracted symmetrical faces | 114 | 20 | 28 | 191 | 985 | 1251 |
| # of extracted symmetric regions | 13 | 2 | 2 | 25 | 14 | 44 |
| Time for symmetry candidate test (Boundary edge lengths and areas) [s] | 0.059 | 0.025 | 0.031 | 0.044 | 1.048 | 0.428 |
| Time for symmetry candidate test (principal curvature histograms) [s] | 0.059 | 0.006 | 0.015 | 0.051 | 0.505 | 0.581 |
| Time for geometric symmetry test [s] | 0.001 | 0.001 | 0.001 | 0.009 | 0.006 | 0.042 |
| Total processing time [s] | 0.119 | 0.032 | 0.047 | 0.104 | 1.559 | 1.051 |
| Per face processing time [s] | $0.92\times10^{-3}$ | $0.86\times10^{-3}$ | $0.28\times10^{-3}$ | $0.38\times10^{-3}$ | $1.2\times10^{-3}$ | $0.66\times10^{-3}$ |

Tab. 1: Model statistics and processing time.

the extracted regions and symmetry surfaces shows that the proposed algorithm can extract representative symmetry regions within each model. Additionally, even though some models have symmetric face pairs with different geometric classes (torus and NURBS surfaces), these regions are correctly extracted as part of the symmetric region, indicating that the proposed algorithm can successfully extract symmetric regions, independent of the geometric class of the faces.

As shown in Tab.1., the total processing time was approximately 1 s for a model with 1598 faces and the per-face processing time was sufficiently fast, ranging from 0.28 to 1.2 ms.

Conclusion:

This study proposed a unified and efficient method to extract reflection-symmetry regions from 3D CAD models, independent of the geometric classes of the faces. The hierarchical filtering of face pairs by comparing only the descriptor values common to all geometric classes of the faces, such as principal curvature distribution, enabled a uniform extraction process, regardless of the geometric class. It was confirmed that symmetric face segment pairs can be extracted even when free-form surfaces are included. The extraction process was sufficiently fast; it took less than a few milliseconds per face.

In our future work, we will extend the method to axisymmetric region extraction and to the case when one face has a symmetric shape with the union of multiple counterpart faces.

*Ren Nakata*, https://orcid.org/0009-0005-6429-9552
*Satoshi Kanai*, https://orcid.org/0000-0003-3570-1782
*Hiroaki Date*, https://orcid.org/0000-0002-6189-2044
*Hideyoshi Takashima*, https://orcid.org/0000-0002-7158-6059
*Tetsufumi Taichi*, https://orcid.org/0009-0006-0748-8303

References:

[1] Buric, M.; Brcic, M.; Bojcetic, N.; Skec S.: Computer-aided detection of exact reflection and axisymmetry in B-rep CAD Models, Computer-Aided Design & Applications, 20(5), 2022, 884-897. https://doi.org/10.14733/cadaps.2023.884-897

[2] Li, C.; Li, M.; Gao, S.: Multi-scale symmetry detection of CAD models, Computer-Aided Design & Applications, 16(1), 2019, 50-66. https://doi.org/10.14733/cadaps.2019.50-66

[3] Li, K.; Foucault, G.; Léon, J.-C.; Trlin, M.: Fast global and partial reflective symmetry analysis using boundary surface of mechanical components, Computer-Aided Design, 53, 2014, 70-89. https://doi.org/10.1016/j.cad.2014.03.005

[4] Mitra, N.-J.; Guibas, L.-J.; Pauly, M.: Partial and approximate symmetry detection for 3D geometry, ACM Transactions on Graphics, 25(3), 2006, 560-568. https://doi.org/10.1145/1141911.1141924

[5] Open CASCADE, OCCT3D collaborative development portal, https://dev.opencascade.org.

[6] žalik, B.; Strnad, D.; Kohek, Š.; Kolingerová, I.; Nerat, A.; Lukač, N.; Podgorelec, D.: A hierarchical universal algorithm for geometric objects reflection symmetry detection, Symmetry, 14(5), 2022, 1060. https://doi.org/10.3390/sym14051060